JOURNAL OF OPTOELECTRONICS AND ADVANCED MATERIALS Vol. 27, Iss. 7 - 8, July - August 2025, p. 342 - 353

Investigation of rhombic block photonic crystal patch antenna for wireless devices with substantial data rates

N. S. YOGA ANANTH[1,*], P. KARUPPASAMY[2]
[1]*Department of Electronics and Communication Engineering, P. S. R. Engineering College, Sivakasi, India*
[2]*Department of Electronics and Communication Engineering, Adithya Institute of Technology,Coimbatore, India*

The next significant development in wireless communication is the shift to 6G technology, which expands upon 5G's innovations and incorporates new features and technologies. 6G is anticipated to reach ultra-high data speeds, possibly in the terabits per second (Tbps) level, by using the terahertz (THz) band (0.1–10 THz). This article explores the distinct design of the Pentagonal edged microstrip patch antenna (PEMPA) structure and examines antenna performance. Further, the structure is embedded with a unique rhombic air-pored photonic crystal (PhC) substrate and simulated using the CST tool. To improve the antenna's performance, the investigation continues to optimize the PhC air hole size and lattice constant value. The proposed unique PhC-based PEMPA achieved remarkable antenna properties, including -77.66 dB (RL), 8.752 dB gain at 2.06 THz, and a high data rate in the Tbps range. The goal of the suggested antenna is to achieve sub-millisecond latency, which is essential for real-time uses in machinery automation, automatic vehicle operation, and robotic surgery.

(Received January 20, 2025; accepted August 5, 2025)

Keywords: Patch antenna, Photonic crystals, Terahertz frequency, Data rate, Bandwidth

1. Introduction

Data transfer rate is an important factor that influences the performance and operation of numerous digital technologies [1, 2] and modern wireless telecommunications [3, 4]. Spectral efficiency, or the effective utilization of a specific bandwidth, directly correlates with the data rate. A higher data rate usually results in a more efficient use of the readily accessible spectrum. In the electromagnetic spectrum [5, 6], Terahertz (THz) or T rays [7–10] have a great deal of promise for wireless communication applications to reach very high data speeds. THz communication offers more transmission capacity, improved secrecy, and more robust anti-interference capability than microwave interaction [11]. When compared to optical communication [12, 13], telecommunication can guarantee the dependability of communications in challenging situations since it has lower photon energy and better smoke and dust penetration. The microstrip patch antenna (MPA) [14–18] is a vital device that contributes significantly to wireless systems because of its low cost, conformance, adaptability, and lightweight nature. The patch's primary disadvantage is that it stimulates surface waves [19], which direct more waves toward the substrate than the air side. Researchers use three methods to alleviate this problem, which lowers antenna performance: PhC [20–23], metamaterials [24–26], and defective ground substrate [27, 28].

The present investigation embraces the PhC concept and demonstrates how the PhC-based MPA may improve antenna efficiency. Emerging PhC technology could hold the key to creating ultra-wideband [29, 30] microstrip antennas. This technology reduces side lobes and electromagnetic interference levels while improving antenna efficiency and bandwidth by totally prohibiting the formation of surface waves with substrate manipulation. While many applications in optics have been proposed in the past, the scalability of these structures also enables their use in the millimeter and THz wave regimes. Electromagnetic crystal materials have garnered significant interest. To increase the energy coupled to the radiated field, replace the dielectric substrate with a PhC crystal with a forbidden gap that includes the antenna excitation frequency and no surface modes. This allows power to be reflected to the air side rather than towards the substrate.

Previous research extensively investigates PhC-based patch antennas to enhance their antenna performances. The existing PhC antenna works are described below: Singh [31] proposed a multifrequency band MPA antenna embedded with cylinder air pores in a in a PhC structure. Partial elimination of bound surface waves within specific directions can maximize the MPA efficiency. For high-efficiency antennas, the energy distribution between space and leaky waves determines the approximate values of directivity and gain. The low directivity of space waves contrasts with the highly directive radiation pattern of leaky waves. To obtain a high-gain antenna, a strong, leaky wave must be excited. The antenna is resonated at different frequencies (0.693, 0.775, 0.794, and 0.852 THz), and the structure yields a high gain of 9 dB at 0.797 THz. Li et al. [32] designed a rectangular patch antenna with a PhC substrate.

The PhC substrate is designed using square and circular air pores with dimensions of 16 mm and 32 mm. The proposed antenna produces excellent results at -31 dB Return Loss (RL) with 5 dB gain. It has been observed that the photonic bandgap (PBG) structure may increase the gain of patch antennas. Consequently, the substrate absorbs less electromagnetic wave energy, reflecting this energy back into free space, thereby significantly improving the return loss and gain. Singh and Singh [33] suggested a trapezoidal patch antenna, and the antenna worked in the frequency range of 1.2–1.6 THz. Surface leaky waves restrict patch antenna performance; therefore, PhC in the thick dielectric substrate improve the patch antenna's workability. There has been a noticeable and significant improvement in the return loss, Voltage standing wave ratio (VSWR), and gain.

Tripathi and Kumar [34] investigated a miniaturized THz antenna with a PBG structure using graphene material. The suggested antenna exhibits superior performance parameters, including lower dimensions and a maximum directivity of 8.42 dB and 7.99 dB for the given antenna. The suggested designs have the potential to be highly helpful in future area-limited applications like Wireless Networks on Chip and Wireless Nano-Sensor Networks, as well as high-speed, short-distance indoor communication. Aloui et al. [35] suggested a wideband THz antenna for biosensor gadgets such as breast tumor detection operated in the 4-6 THz terahertz range. Graphene's high conductivity allows for a characteristic improvement over copper. Additionally, the use of PBG structure at the substrate level and SIW technology improved the antenna's performance.

Danasegaran et al. [36] investigated a patch antenna for 5G communication, as well as the concept of PBG. The authors of this paper chose a triangular lattice structure to make a PhC-based patch antenna. At 1.59 THz, the antenna showed -31 dB RL and 2.8 dBi directivity. The PhC patch antenna structure incorporates the line defect concept to enhance its performance. The final results show that the defected PhC produces excellent characteristics due to the trapping of EM waves into the pores and reflective walls. Youssef et al. [37] proposed a PBG antenna that resonates within the frequency band of 0.3–1.25 THz. The results show a significant increase in bandwidth as well as gain. PBG is a very promising alternative for terahertz imaging systems, such as those used to find hidden items in places like airports, because of its unique qualities and the antenna's multiband capabilities. Biological imaging can also benefit from its promise, as it can enhance the clarity and contrast of tissue abnormalities.

Pandian et al. [38] studied the hourglass patch antenna based on PhC substrate for the application of breast cancer. Because of its non-ionizing properties, the suggested antenna resonated at the THz frequency, which is safer and has no effect on human health. The proposed PhC structure is small, less costly, lightweight, ecologically safe, and can serve as the primary screening method for individuals with breast cancer, especially in resource-constrained areas. Li et al. [39] explored the high-gain THz antenna with a rectangular polyimide dielectric column for the PBG substrate. The PBG antenna may achieve tri-band operational characteristics by utilizing PBG and polyimide substrates in a multilayer substrate configuration. Additionally, at the three operational bands, the PBG antenna's radiation efficiencies are above 93%, 92%, and 88%, respectively. These are marginally greater than those of the H antenna and superior to those of the dominant multi-band antenna. The above survey data shows that there are more PhC-based patch antennas existing presently, whereas their antenna performances are poor. Moreover, the existing patch shape is conventional, and the PhC air hole is regular. As a result, this paper focuses on the unique patch of the antenna structure, such as a pentagonal-edged MPA. The pentagonal structure is embedded in the corners and the mid-face of the square patch antenna structure. Along with that, the PhC structure is designed with unique rhombic-shaped air pores rather than regular cylindrical air holes. The antenna patch's distinctive forms and PhC air holes can improve antenna performance in areas such as return loss, bandwidth, directivity, VSWR, directivity, and gain. Section 2 elucidates the proposed PEMPA design, while Section 3 delves into the PhC structure and design. Section 4 explains the influence of the lattice constant on the rhombic air-hole PhC structure. Section 5 compares and analyzes the proposed PEMPA structures, while Section 6 concludes the work.

2. Proposed pentagonal edged microstrip patch antenna (PEMPA) design

MPA's fundamental structure comprises the radiating patch, dielectric substrate, and ground layer. The substrate is chosen depending on the specifications, whereas the layers of patch and ground can be constructed of either copper or gold. This particular design uses Roger 3003 as the substrate and copper for the patch and ground layers. Rogers RO3003 is perfect for high-frequency, high-efficiency antenna applications owing to its low dielectric constant, ultra-low loss tangent, and good thermal and electrical stability. There would be a rise in dielectric losses, a degradation in gain and bandwidth, and performance volatility caused by moisture or temperature effects if a higher-loss or higher-εr material were to be used in its place. This paper proposes and designs the unique PEMPA structure in three different ways, starting with the square patch antenna as illustrated in Fig. 1(a). Further, the structure is modified with a pentagonal model in each corner of the square patch. Fig. 1(b) displays the pentagon-embedded squared patch structure. Finally, the PEMPA structure is obtained by embedding three pentagons in the midpoint of the square patch, as illustrated in Fig. 1(c). Hence, the proposed PEMPA structure is designed by embedding seven pentagonal structures in the midpoint and corner of the square patch antenna. The dimension of the proposed PEMPA antenna is calculated using the below formulas and the values are illustrated in Table 1.

$$W = \frac{c_{\mathrm{VL}}}{2f_{OP}}\sqrt{\frac{2}{\varepsilon_r+1}} \tag{1}$$

$$L = \frac{c_{\mathrm{VL}}}{2f_{op}\sqrt{\varepsilon_{reff}}} - 2\Delta L \tag{2}$$

The outcomes of the proposed conventional MPA structures are highlighted in Table 2. The RL comparison of the distinct three structures is shown in Fig. 2. It is inferred that the third (PEMPA) structure produces better characteristics.

Table 1. Proposed PEMPA dimensions

Parameters	Ground		Substrate			Patch			Feed	
	length	width	length	width	height	length	width	Thickness	length	width
Dimension (μm)	142.5	142.5	142.5	142.5	4.5	78.5	78.5	12	32	13.70

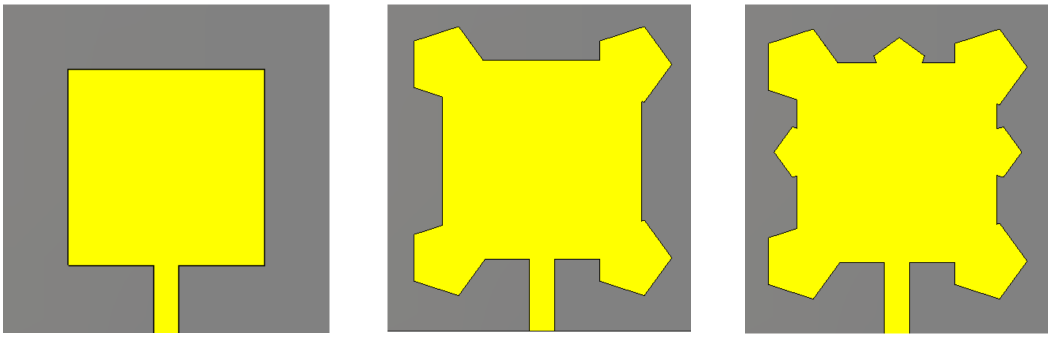

Fig. 1. Proposed PEMPA (a) Structure 1 (b) Structure 2 (c) Structure 3 (colour online)

Table 2. Performance of proposed three different MPAs

Design/Parameters	Freq. (THz)	RL (dB)	VSWR	Gain (dB)	Directivity (dBi)	Bandwidth (THz)
Antenna structure 1	2.026	-32.79	1.5489	4.281	4.764	0.075
Antenna structure 2	2.035	-37.82	1.4380	4.816	4.937	0.082
Antenna structure 3	2.042	-40.08	1.3023	5.270	5.481	0.094

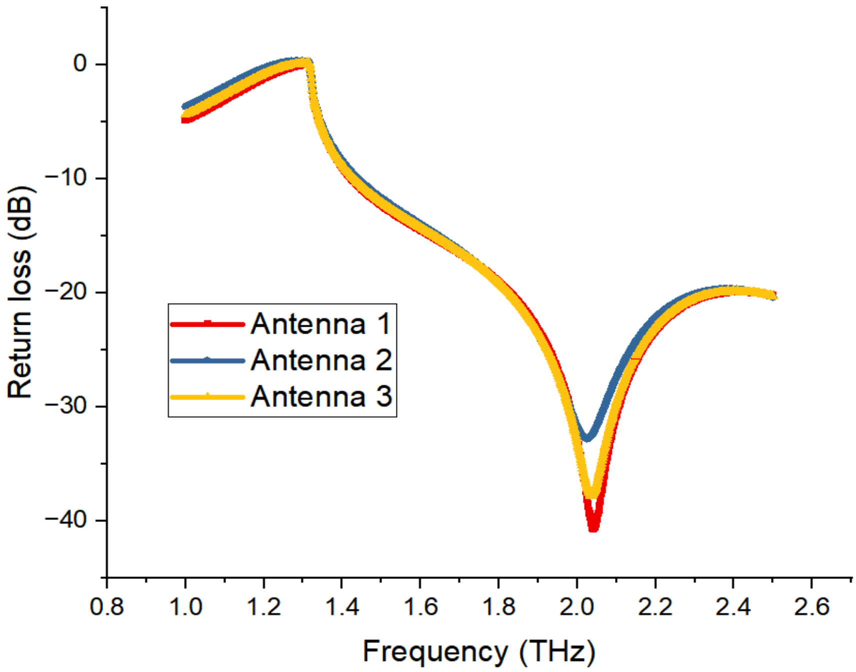

Fig. 2. RL Comparison of proposed three MPAs (PEMPA) (colour online)

3. Proposed PhC structure and design

PhC is an organic structure characterized by sporadic refractive index variations. PhC, also known as a PBG [40, 41], consists of orthogonally bored low dielectric constant air holes into strong dielectric material, completely preventing EM wave passage for frequency selection in both directions. In a homogeneous dielectric medium, the mode is on the light path, and the speed of light falls with refractive index. A PhC's dielectric constant fluctuates sporadically in all directions of space. The design of PhC involves three different dimensions. This paper prefers to design the antenna structure using 2D PhC. There are two distinct topologies for the 2D PhC: hole and rod types. The hole pattern [42] of PhC, with a filling factor of over 50%, primarily consists of semiconductor material and features a pattern of low-indexed air-filled pores set against a background of high-index material. PhC has a filling factor [43] of beneath fifty percent and contains low-index surface material around the highly indexed rods.

The size of the air holes in a PhC is an important factor that affects its PBG, effective refractive index, and other optical properties. Generally, the design of a PBG involves circular air holes, but this paper chooses the unique rhombus-shaped airhole to analyze the PBG structure. Different periodic arrangements, including square, triangular, honeycomb, and aperiodic architectures, can be used to categorize PhC topologies. The bandgap properties and mode confinement behaviour are defined by these topologies. A square lattice topology is typically chosen for microwave and patch antenna designs because of its straightforward design, efficient surface wave suppression, and simplicity in integrating with planar production techniques. Wider bandgaps may be possible with triangular lattices, but square lattices with manufactured flaws are a more feasible option for improving antenna performance due to their complexity and manufacturing requirements. The present section explores several antenna models by varying the size of rhombic air holes in square lattice PEMPA structures. Therefore, the PEMPA structure is designed by varying the air-hole size from 2 μm to 10 μm. The effective permittivity and permeability of an air hole might change depending on its size. Fig. 3 (a-e) illustrates the various antenna arrangements. The radius modifications produce the highest bandgap by reducing the vein breath in the PBG, leading to a TE mode gap and a significant amount of TM [44] mode. This improves the localized electromagnetic wave's resonance intensity.

Table 3 highlights the antenna performances for various sizes of rhombic air holes. It is observed that the antenna resonant frequencies range between 2.041 – 2.063 THz due to distinct airhole sizes. Fig. 4 depicts RL's impact on various air hole sizes. The minimum RL value (-77.66 dB) is attained for the PEMPA structure with an air hole size of 4 μm, and a maximum RL of -39.06 dB is achieved for the structure of 10 μm. Fig. 5 (a and b) show the influence of VSWR and gain characteristics for various rhombic air hole sizes.

The photonic crystal-based antenna outperforms conventional microstrip designs by using bandgap features to suppress surface waves, resulting in increased radiation efficiency, bandwidth, and gain. The periodic shape improves impedance matching and channels more radiated energy to the primary lobe, minimising side lobes and back radiation. As a result, the PhC antenna exhibits excellent efficiency and pattern stability, especially in high-frequency applications

4. Impact of lattice constant of Rhombic air-hole PhC structure

Generally, the design of PhC involves two distinct structures: square and triangular lattices [45-47]. Total internal reflections, resulting from the strong index contrast over the high and low index surfaces, govern the light localization in the PhC slab. Conversely, the two-dimensional PhC structure's distributed Bragg reflector governs the longitudinal confinement. This article assumes a square lattice PhC structure for future investigation. In this section, the lattice constant values of the PhC structure are optimized in the range of 12–22 μm to analyze the antenna characteristics. Fig. 6 (a–e) shows the proposed PEMPA structure for distinct lattice constant values. For the proposed PEMPA structures with a lattice dimension of 6 μm, the substrate has 57 air-holes. The quantity of air holes reduces when lattice values are steadily increased. Table 4 lists the performances of the PhC structures at various lattice values. Fig. 7 compares and illustrates the RL parameters for different proposed structures. The impact of VSWR and gain of the various lattice constants is illustrated in Fig. 8. It is observed that the PEMPA structure with a lattice value of 16 μm produces enhanced outcomes with a maximum directivity of 8.7 dBi.

5. Comparison of traditional and optimized PhC PEMPA

This section compares and analyze the performances of the proposed traditional and optimized PhC PEMPA structures. Fig. 9 illustrates the proposed PEMPA and optimized PhC structures. At 2.04 THz, the traditional PEMPA structure produces a result of -40.08 dB RL with 5.27 dB gain. We further optimize the PEMPA structure for different rhombic air hole sizes and lattice constant values.

At 2.06 THz, the optimized PhC PEMPA structure yields -77.66 dB RL and 8.752 dB gain. Table 5 lists the proposed structures' various performances. The conventional antenna produces the average antenna performances due to leaky wave issues. It is overcome by adopting PhC structure and the RL performance is improved upto 83.8%, gain is enhanced till 66% and bandwidth is boosted around 250%. It is due to Periodic modulation in PhC structures can cause some guided modes to transform into leaky waves. These leaky modes can emit energy into free space at regulated angles because they are not completely enclosed. PhCs are therefore perfect for directed radiation and beam shaping.

Fig. 10 presents the RL comparison of the proposed PEMPA structures, revealing that the PhC PEMPA generates an enhanced output. Fig. 11 shows the 1D and 3D of the proposed PEMPAs and the H field and surface current distribution of the proposed PhC structure is illustrated in Fig. 12. Antenna H-field distribution shows that magnetic loops are concentrated in the dielectric, particularly under the patch, and that fringing effects make them greatest at the edges. A dense concentration of current surrounding the feed and the margins of the altered patch is visible in the surface current distribution, suggesting longer electric paths. The corner adjustments' uneven current flow helps to widen the bandwidth and may even allow for multi-mode operation.

The results demonstrate that extending the non-transmission frequency range allows the PhC with heterostructures to operate in a wider working frequency band than conventional patch antennas. Furthermore, it may significantly increase both its return loss and radiation efficiency. The PBG is responsible for suppressing surface waves that propagate over the substrate's surface and considerably reflecting the majority of electromagnetic wave energy transmitted to the substrate. Because of these advantages, PhC antennas will become more common in a variety of applications, including satellite and mobile communications, as well as communications related to astronautics and aeronautics.

Since the suggested PEMPA structure is built for the THz frequency, its supported wavelength is in the micrometer range. The antenna size is proportionate to wavelength, indicating that this antenna has a miniaturized construction. This confirms that the suggested antenna would use less power while fulfilling the functions of a transmitter and receiver. Problems with fast data rates and low power consumption may be readily handled if wireless equipment, such as sensors, is designed to operate in the THz frequency range. A bigger bandwidth (B) allows for a higher maximum data throughput, assuming constant SNR.

In reality, as bandwidth grows, more symbols/second may be broadcast, allowing for higher-order modulation.

$$\text{Data rate} \leq B \log2 (1+\text{SNR}) \tag{3}$$

Metamaterials and photonic crystals are both artificial sequential structures, although their size and functioning are different. A photonic crystal's unit cell size is proportional to its wavelength, and it uses Bragg scattering and photonic bandgaps to control electromagnetic waves. In contrast, metamaterials can attain unusual effective characteristics like as negative permittivity or permeability by means of subwavelength resonant structures. In order to increase radiation control, enhance bandwidth, and suppress surface waves, the author opted for the PhC method, which has low-loss bandgap [48, 49] features. The proposed result is compared with existing PhC work which is listed in Table 6. It is inferred that the proposed PhC antenna outcome is much better than others due to its unique patch and air hole in PhC structure.

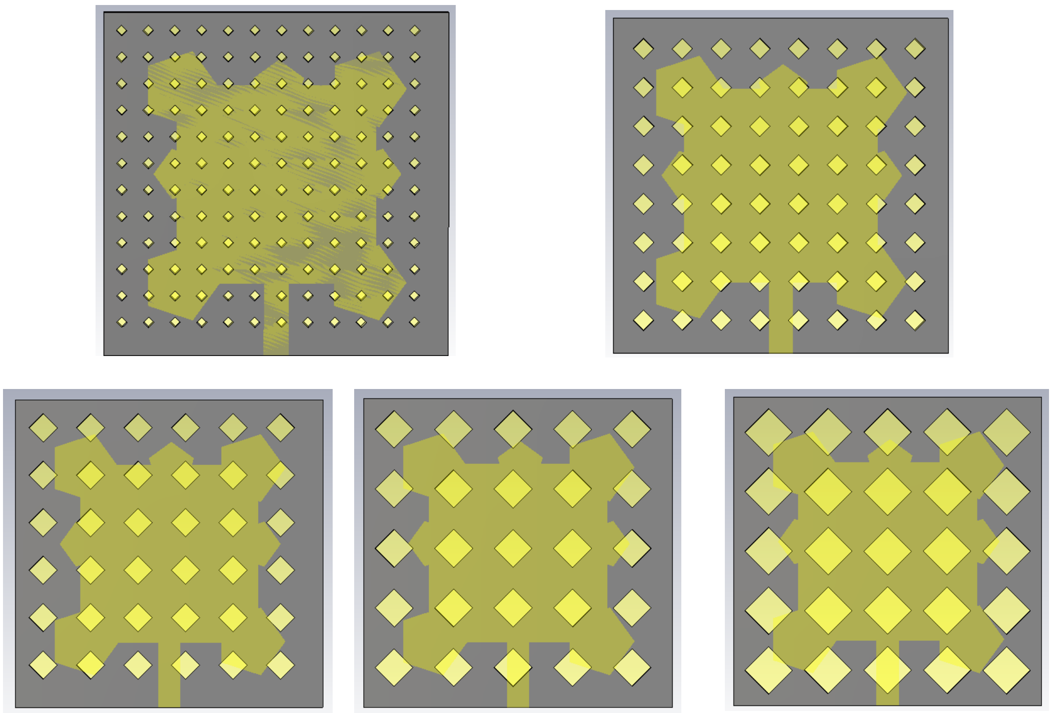

Fig. 3. Proposed PEMPA for different rhombic airhole size (colour online)

Table 3. Influence of rhombic air holes size on PEMPA

Rhombus air hole sizes (μm) / Parameters	Freq. (THz)	RL (dB)	VSWR	Gain (dB)	Directivity (dBi)	Bandwidth (THz)
2	2.048	-45.19	1.0310	7.252	8.467	0.228
4	2.063	-77.66	1.0110	8.752	8.767	0.328
6	2.063	-53.25	1.0278	8.155	8.270	0.243
8	2.059	-45.98	1.0298	6.921	7.204	0.210
10	2.041	-40.38	1.0211	6.489	6.702	0.217

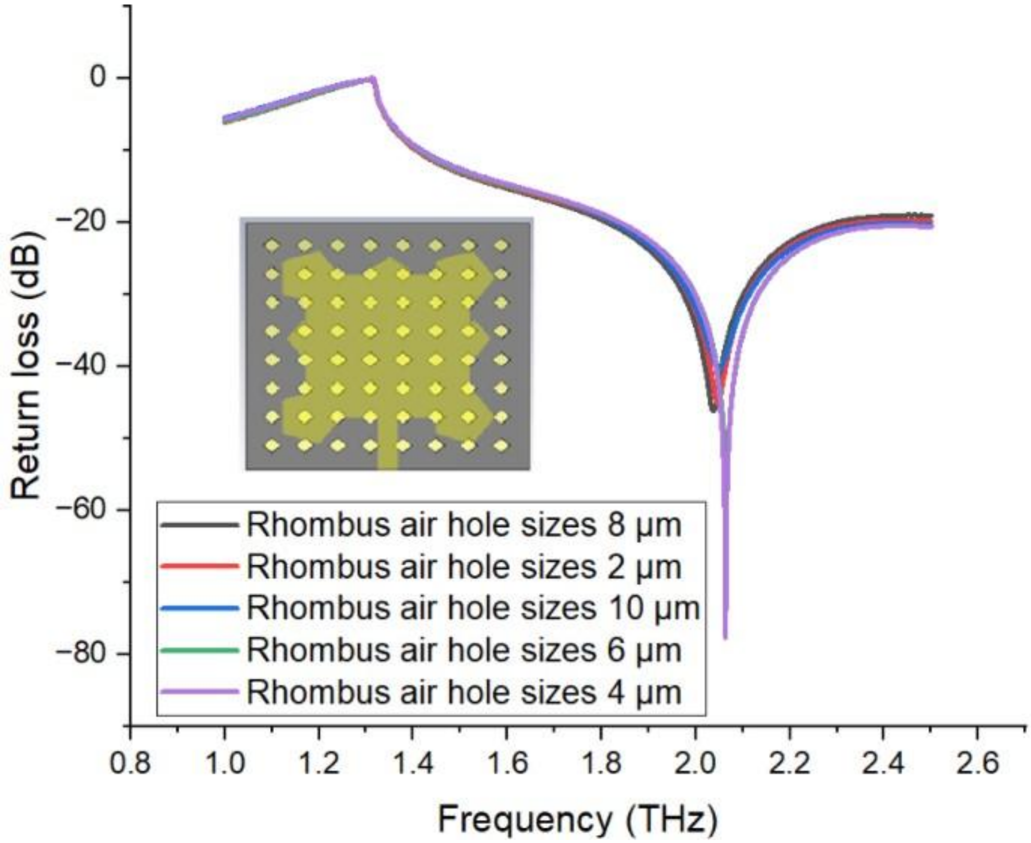

Fig. 4. RL Comparison of distinct rhombic air hole size (colour online)

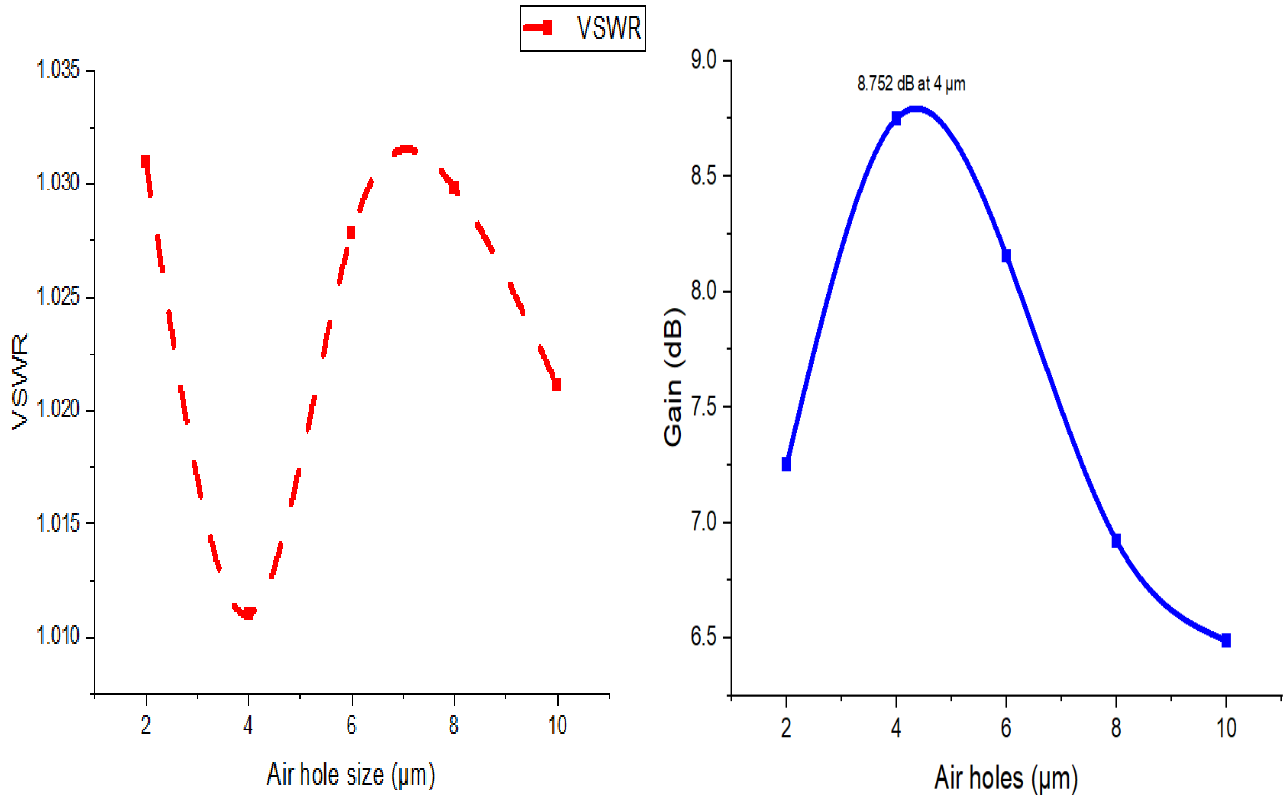

Fig. 5. (a) Impact of VSWR vs air hole size (b) Impact of gain vs air hole size (colour online)

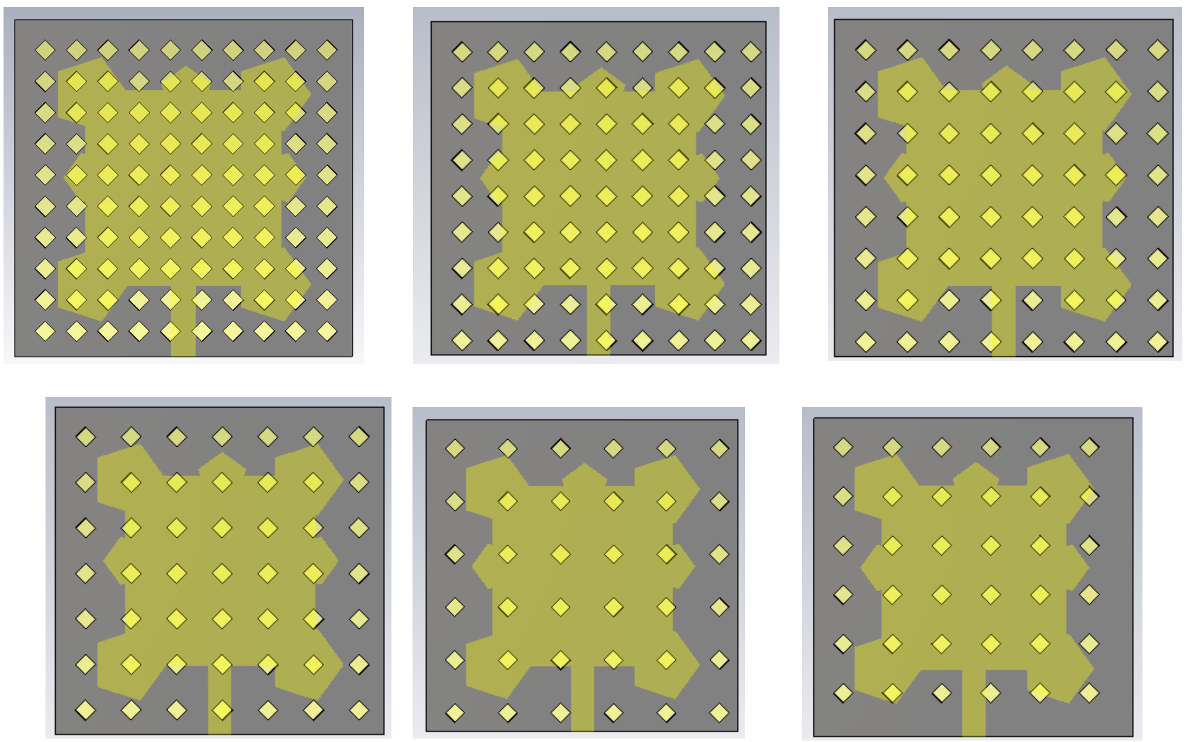

Fig. 6. Proposed PEMPA structure for various lattice constant values (colour online)

Table 4. Influence of lattice constant values on PEMPA (colour online)

Rhombus air hole lattice constant / Parameters	Freq. (THz)	RL (dB)	VSWR	Gain (dB)	Directivity (dBi)	Bandwidth (THz)
12	2.062	-45.24	1.0365	6.892		
14	2.068	-50.19	1.0318	7.204		
16	2.063	-77.66	1.0110	8.752	8.767	0.328
18	2.0365	-38.68	1.0235	8.026		
20	2.0365	-37.92	1.0557	7.575	8.884	
22	2.0365	-39.48	1.0414	7.412		

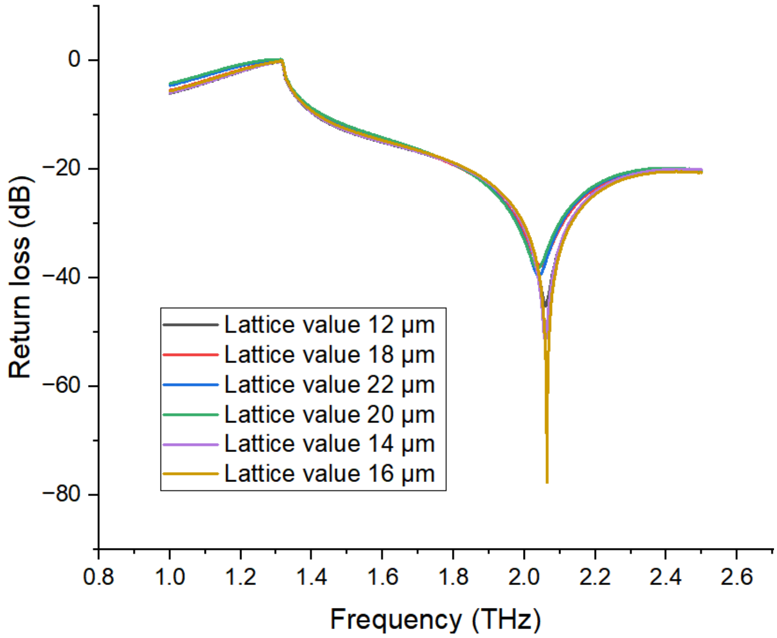

Fig. 7. RL Comparison of RL for distinct lattice constant (colour online)

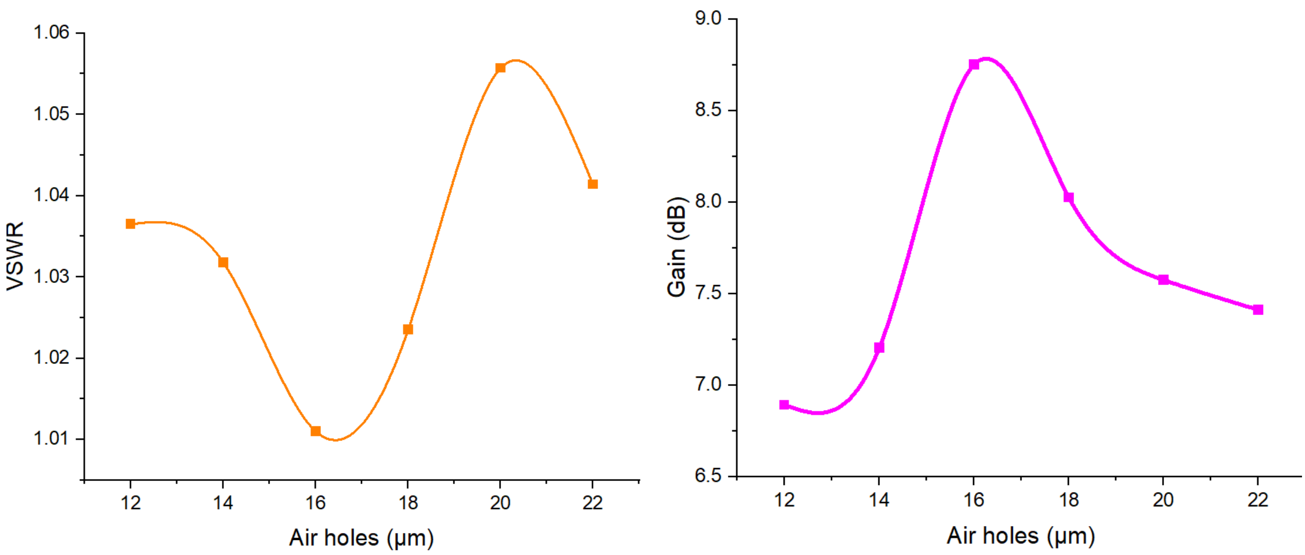

Fig. 8. (a) Impact of VSWR vs lattice values (b) Impact of gain vs lattice values (colour online)

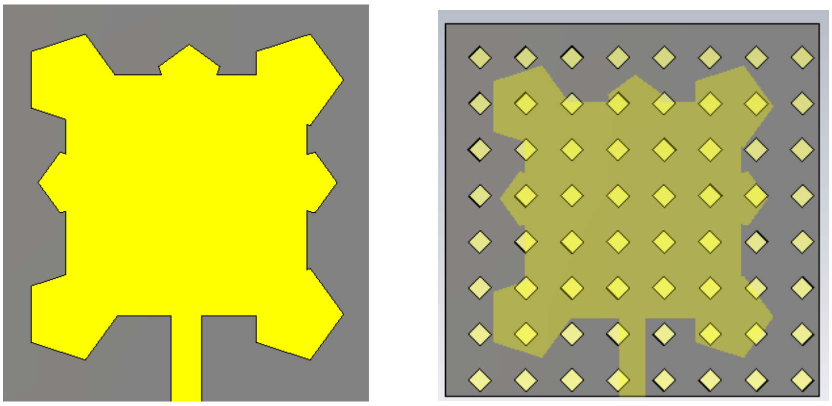

Fig. 9. (a) Conventional PEMPA (b) PhC based PEMPA (colour online)

Table 5. Comparison of traditional and PhC PEMPA performances

Proposed design/Parameters	Freq. (THz)	RL (dB)	VSWR	Gain (dB)	Directivity (dBi)	Bandwidth (THz)
Traditional PEMPA	2.042	-40.08	1.3023	5.270	5.481	0.094
PhC PEMPA	2.063	-77.66	1.0110	8.752	8.767	0.328
Enhancement (%)	-	83.83	-	66.07	59.95	248.94

Table 6. Comparison of PEMPA performances with existing works

Proposed design/Parameters	Proposed work	Ref. [36]	Ref. [37]	Ref. [38]	Ref. [50]	Ref. [51]
Freq. (THz)	2.063	1.58	1.13	1.55	2.04	4
RL (dB)	-77.66	-50.60	-41.81	-33.78	-71.35	<-10
Gain (dB)	8.752	-	9.4	-	9.5	7.8

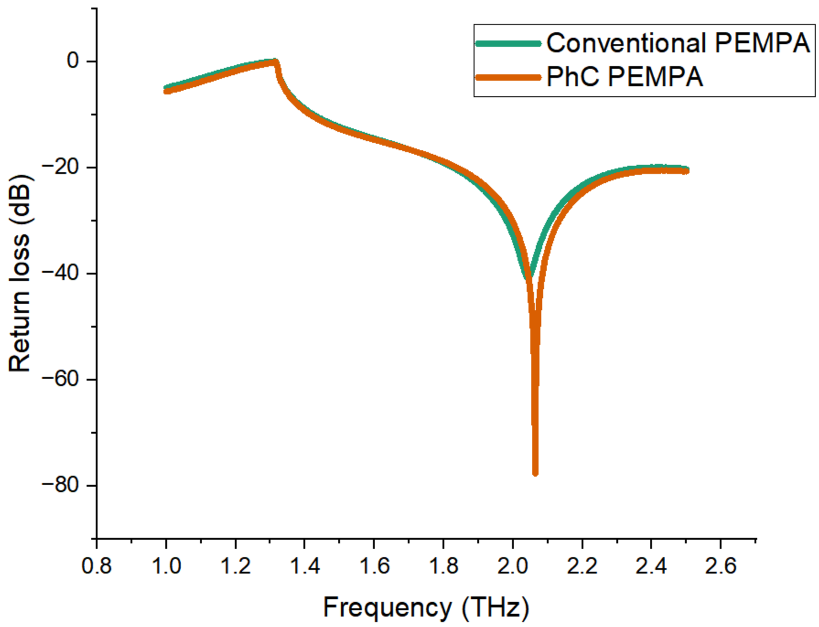

Fig. 10. RL comparison plot of conventional and PhC PEMPAs (colour online)

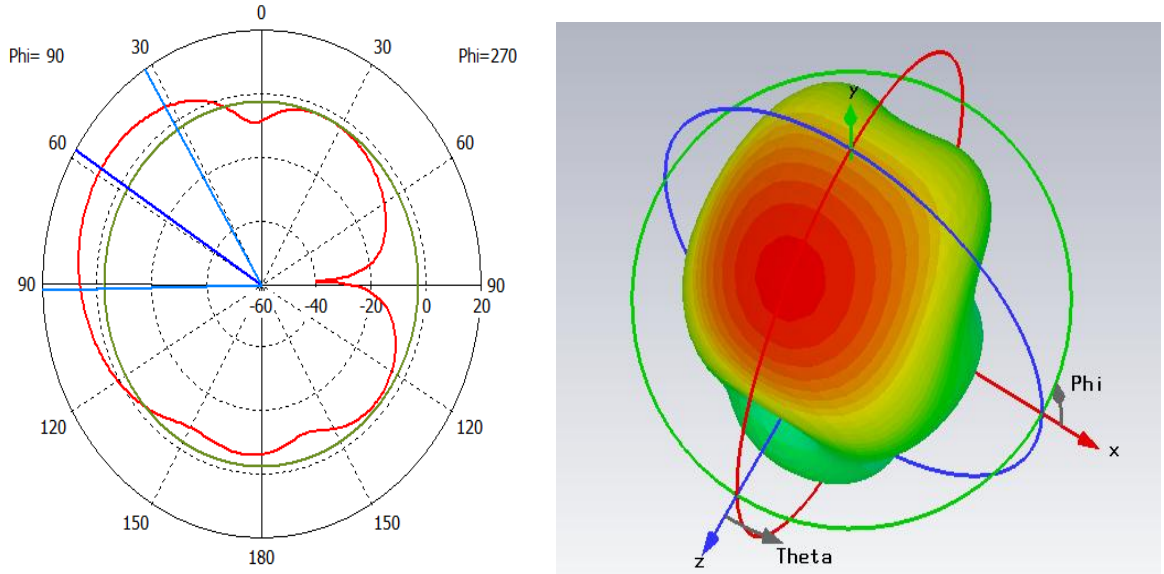

Fig. 11. (a) 1 D (b) 3D view of Directivity plot of PhC PEMPA (colour online)

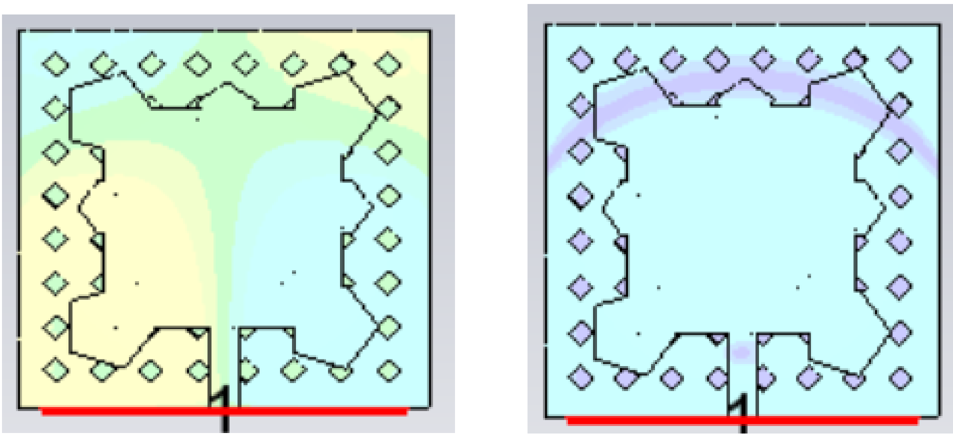

Fig. 12. (a) H field (b) Current distribution of PEMPAs (colour online)

6. Conclusion

This article examined the impact of PhC on the patch antenna structure with its unique rhombic air pores. The rhombic air pores are drilled into the square lattice substrate in the size of an 8 x 8 matrix structure. The proposed PhC antenna is optimized by two distinct parameters: air pore size and lattice constant values. The proposed unique PhC-based PEMPA attained outstanding antenna characteristics of -77.66 dB RL and 8.752 dB gain at 2.06 THz, whereas the conventional PEMPA structure delivered -40.08 dB RL with 5.27 dB gain at 2.04 THz frequency. Every wireless device relies heavily on data rate, and the suggested antenna's bandwidth is closer to Tbps. The suggested PEMPA structure offers the highest data rate and is therefore appropriate for a range of wireless devices and THz applications, including the biomedical industry.

References

[1] Tommaso Ciarli, Martin Kenney, Silvia Massini, Lucia Piscitello, Research Policy **50**(6), 104289 (2021).
[2] Jaume Anguera, Aurora Andújar, Minh Chau Huynh, Charlie Orlenius, Cristina Picher, Carles Puente, International Journal of Antennas and Propagation **2013**, 838364 (2013).
[3] International Telecommunication Union, Technology Trends of Active Services in the Frequency Range 275–3000 GHz; Recommendation ITU-R, Document SM.2352-0; International Telecommunication Union: Geneva, Switzerland, 2015
[4] Radha Raman Chandan, Awatef Balobaid, Naga Lakshmi Sowjanya Cherukupalli, H. L. Gururaj, Francesco Flammini, Rajesh Natarajan, Electronics **12**(5), 1095 (2023).

[5] C. A. Balanis, Advanced Engineering Electromagnetics, John Wiley & Sons, Inc.: Hoboken, NJ, USA, 1989.
[6] J. Zimmerling, L. Wei, P. Urbach, R. Remis, J. Comput. Phys. **315**, 348 (2016).
[7] R. Piesiewicz, T. Kleine-Ostmann, N. Krumbholz, D. Mittleman, M. Koch, J. Schoebel, T. Kurner, IEEE Antenn. Propag. M. **49**(6), 24 (2007).
[8] M. Matsuura, M. Tani, K. Sakai, Appl. Phys. Lett. **70**, 559 (1997).
[9] E. C. Britto, S. K. Danasegaran, K. Sagadevan, K. (2023). Performance Analysis of SSRR in High-Speed Terahertz Antenna for Biomedical Applications, in S. Mehta, A. Abougreen (Eds.), Metamaterial Technology and Intelligent Metasurfaces for Wireless Communication Systems, IGI Global, 180 (2023).
[10] M. Tamagnone, J. S. Gómez-Díaz, J. R. Mosig, J. Perruisseau-Carrier, J. Appl. Phys. **112**, 114915 (2012).
[11] F. Monticone, A. Alù, Proc. IEEE **103**, 793 (2015).
[12] K. D. Paschaloudis, C. L. Zekios, G. C. Trichopoulos, F. Farmakis, G. A. Kyriacou, Electronics **10**, 2782 (2021).
[13] G. S. Unal, M. I. Aksun, Sci. Rep. **5**, 15941 (2015).
[14] A. D. Dhillon, D. Mittal, E. Sidhu, Optik **144**, 634 (2017).
[15] A. Sharma, G. Singh, J. Infrared Millim. Terahertz Waves **30**, 1 (2008).
[16] S. K. Danasegaran, E. C. Britto, S. Dhanasekaran, G. Rajalakshmi, S. Lalithakumari, A. Sivasangari, G. Sathish Kumar, G. (2024). Design and Investigation of Line-Defected Photonic Crystal Antenna for Outstanding Data Transmission, in S. Mehta & Rupesh Kumar (Eds.), Radar and RF Front End System Designs for Wireless Systems, IGI Global, 176 (2024).
[17] A. Sharma, G. Singh, J. Infrared Milli. Terahz. Waves **30**, 1 (2009).
[18] D. M. Pozar, Proc. IEEE **80**(1), 79 (1992).
[19] R. Gonzalo, P. De Maagt, M. Sorolla, IEEE Transactions on Microwave Theory and Techniques **47**(11), 2131 (1999).
[20] E. Yablonovitch, J. Modern Opt. **41**(2), 173 (1994).
[21] G. Rajalakshmi, S. K. Danasegaran, R. Pandian, S. Lalithakumari, Opt. Quant. Electron. **56**, 1282 (2024).
[22] Z. Liqiang, Z. Chenxi, Y. Sicheng, Z. Zhuoran, G. Daohan, Res. Phys. **31**(4), 105054 (2021).
[23] R. K. Kushwaha, P. Karuppanan, L. D. Malviya, Physics B Condensed Matter **545**, 107 (2018).
[24] A. Vahdati, F. Parandin, Wireless Personal Communications **109**(4), 2213 (2019).
[25] A. Armghan, K. Aliqab, M. Alsharari, O. Alsalman, J. Parmar, S. K. Patel, Micromachines **14**(7), 1328 (2023).
[26] K. Hossain, T. Sabapathy, M. Jusoh, S.-H. Lee, K. S. Ab Rahman, M. R. Kamarudin, Sensors **22**(4), 1626 (2022)
[27] N. AuliaYusuf, P. Dewi Purnamasari, F. Y. Zulkifli, 6th International Conference on Information Technology, Information Systems and Electrical Engineering (ICITISEE), Yogyakarta, Indonesia, 688 (2022).
[28] M. K. Khandelwal, B. K. Kanaujia, S. Dwari, S. Kumar, A. K. Gautam, AEU - Intemational Journal of Electronics and Communications **69**, 39 (2015).
[29] S. Singhal, Microwave and Optical Technology Letters **61**(10), 2366 (2019).
[30] S. N. Mahmood, A. J. Ishak, T. Saeidi, A. C. Soh, A. Jalal, M. A. Imran, Q. H. Abbasi, Micromachines **12**, 322 (2021).
[31] G. Singh, Infrared Physics and Technology **53**(1), 17 (2010).
[32] Zhenghua Li, Yan Ling Xue, Tinggen Shen, Mathematical Problems in Engineering **2012**, 151603 (2012).
[33] A. Singh, S. Singh, Photonics and Nanostructures – Fundamentals and Applications **14**, 52 (2015).
[34] Subodh Kumar Tripathi, Ajay Kumar, Australian Journal of Electrical and Electronics Engineering **16**(2), 74 (2019).
[35] Radhoine Aloui, Hassen Zairi, Fermin Mira, Ignacio Llamas-Garro, Sofien Mhatli, Sensing and Bio-Sensing Research **38**, **100511** (2022).
[36] Sathish Kumar Danasegaran, Elizabeth Caroline Britto, K. Sagadevan, M. Paranthaman, S. Poonguzhali, Mahendran Krishna Kumar, Brazilian Journal of Physics **54**, 31 (2024).
[37] Amraoui Youssef, Imane Halkhams, Rachid El Alami, Mohammed Ouazzani Jamil, Hassan Qjidaa, Results in Engineering **22**, 102327 (2024).
[38] R. Pandian, S. K. Danasegaran, S. Lalithakumari, G. Rajalakshmi, G. Sathish Kumar, Optical and Quantum Electronics **56**, 763 (2024).
[39] G. Li, C. Huang, R. Huang, B. Tang, J. Huang, J. Tan, N. Xia, H. Cui, Photonics **11**, 307 (2024).
[40] M. P. Kesler, Microwave Opt. Technol. Lett. **11**(4), 169 (1996).
[41] M. M. Sigalas, R. Biswas, K. Ho, Microwave Opt. Technol. Lett. **13**(4), 205 (1996).
[42] Qifa Liu, Minjia Meng, Shang Ma, Meixin Feng, Opt. Express **31**, 43615 (2023)
[43] Avi Klein, Inbar Sibony, Sara Meir, Hamootal Duadi, Michelle Y. Sander, Moti Fridman, Applied Photonics **5**(9), 090801 (2020).
[44] J. Kołacz, H. G. Gotjen, R. Y. Bekele, J. D. Myers, J. A. Frantz, M. Ziemkiewicz, C. M. Spillmann, Liquid Crystals **47**(4), 531 (2019).
[45] T. Sridarshini, S. Indira Gandhi, Laser Phys. **30**, 026205 (2020).
[46] K. Mahendran, H. Sudarsan, S. Rathika, AEU - International Journal of Electronics and Communications **161**, 154543 (2023).
[47] K. Mahendran, Sathish Kumar Danasegaran, R. Indhu, S. Annie Angeline Preethi, J. Optoelectron. Adv. M. **26**(3-4), 106 (2024).
[48] Nila Bagheri, Jon Peha, Fernando Velez, Radio Science **60**(5), RS008072 (2025).

[49] M. Sultana, T. Karim, M. A. Alim, A Microstrip Patch Antenna with High Gain for WiMAX and X-Band Applications, 4th International Conference on Robotics, Electrical and Signal Processing Techniques (ICREST), Dhaka, Bangladesh, 60 (2025).
[50] S. K. Danasegaran, L. Swaminathan, A. K. Vaithilingam, A. Sivasangari, J. Nanophoton. **18**(4), 046010 (2024).
[51] G. L. P. Ashok, G. V. Nath, B. C. Neelapu, Appl Opt. **63**(13), 3609 (2024).

*Corresponding author: yogaananthnspsr@gmail.com